Neurobiology of Disease 182 (2023) 106126

Contents lists available at ScienceDirect

Neurobiology of Disease

journal homepage: www.elsevier.com/locate/ynbdi

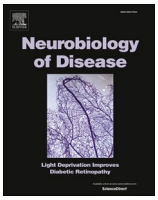

Dual truncation of tau by caspase-2 accelerates its CHIP-mediated degradation

Lydia Reinhardt [a,b], Fabrizio Musacchio [c], Maria Bichmann [a], Annika Behrendt [a], Ebru Ercan-Herbst [a], Juliane Stein [b,1], Isabelle Becher [d], Per Haberkant [d], Julia Mader [b], David C. Schöndorf [a,b], Melanie Schmitt [b], Jürgen Korffmann [b], Peter Reinhardt [b], Christian Pohl [b], Mikhail Savitski [d], Corinna Klein [b], Laura Gasparini [b], Martin Fuhrmann [c], Dagmar E. Ehrnhoefer [a,b,*]

[a] BioMed X Institute, Im Neuenheimer Feld 515, 69120 Heidelberg, Germany
[b] AbbVie Deutschland GmbH & Co. KG, Neuroscience Discovery, Knollstrasse, 67061 Ludwigshafen am Rhein, Germany
[c] Neuroimmunology and Imaging Group, German Center for Neurodegenerative Diseases (DZNE), Venusberg-Campus 1, Building 99, 53127 Bonn, Germany
[d] European Molecular Biology Laboratory (EMBL), Meyerhofstraße 1, 69117 Heidelberg, Germany

ARTICLE INFO

Keywords:
Tau
Caspase-2
Proteolysis
Tauopathy
Degradation
CHIP
Ubiquitination

ABSTRACT

Intraneuronal aggregates of the microtubule binding protein Tau are a hallmark of different neurodegenerative diseases including Alzheimer's disease (AD). In these aggregates, Tau is modified by posttranslational modifications such as phosphorylation as well as by proteolytic cleavage. Here we identify a novel Tau cleavage site at aspartate 65 (D65) that is specific for caspase-2. In addition, we show that the previously described cleavage site at D421 is also efficiently processed by caspase-2, and both sites are cleaved in human brain samples. Caspase-2-generated Tau fragments show increased aggregation potential *in vitro*, but do not accumulate *in vivo* after AAV-mediated overexpression in mouse hippocampus. Interestingly, we observe that steady-state protein levels of caspase-2 generated Tau fragments are low in our *in vivo* model despite strong RNA expression, suggesting efficient clearance. Consistent with this hypothesis, we find that caspase-2 cleavage significantly improves the recognition of Tau by the ubiquitin E3 ligase CHIP, leading to increased ubiquitination and faster degradation of Tau fragments. Taken together our data thus suggest that CHIP-induced ubiquitination is of particular importance for the clearance of caspase-2 generated Tau fragments *in vitro* and *in vivo*.

1. Introduction

Tau is the major component of the proteinaceous aggregates found in multiple neurodegenerative diseases including Alzheimer's disease (AD). In AD, Tau aggregates form neurofibrillary tangles (NFTs), and consist of Tau proteoforms heavily modified by posttranslational modifications (PTMs). On soluble Tau protein, PTMs can be reversible such as phosphorylation or irreversible like proteolysis (Quinn et al., 2018). Proteolytic events may be part of physiological Tau degradation, but they may also render Tau more aggregation-prone, since removal of both the N- and C- termini exposes the aggregation-prone repeat domain region of the protein (Jeganathan et al., 2006; Strooper, 2010). However, the importance of specific Tau truncation events for the formation of NFTs in AD patients remains unclear.

Both the N- and C-termini of Tau can be cleaved by members of the caspase family of proteases, and this cleavage has been associated with the formation of Tau aggregates (Calignon et al., 2010; Mead et al., 2016; Rissman et al., 2004). Caspase-6 has been shown to cleave Tau at D13 (Horowitz et al., 2004), and more recently caspase-2-mediated cleavage at D314 has been reported (Zhao et al., 2016). The caspase cleavage site in Tau that has been studied most extensively is D421, which has been described as a caspase-3 site but may also be cleaved by caspases −6, −7 and −8 (Gamblin et al., 2003; Horowitz et al., 2004).

The ubiquitin E3 ligase carboxyl-terminus of Hsc70 interacting

* Corresponding author at: AbbVie Deutschland GmbH & Co. KG, Neuroscience Discovery, Knollstrasse, 67061 Ludwigshafen am Rhein, Germany.
E-mail address: dagmar.ehrnhoefer@abbvie.com (D.E. Ehrnhoefer).
[1] Former AbbVie employee, current address: CSL Behring Innovation GmbH, Pharmacology & Toxicology, Research Marburg, Michelbacher Strasse, 35041 Marburg, Germany.

https://doi.org/10.1016/j.nbd.2023.106126
Received 9 December 2022; Received in revised form 30 March 2023; Accepted 12 April 2023
Available online 20 April 2023

protein (CHIP) is highly expressed in tissues with terminally differentiated cells and high metabolic activity such as the brain (Paul and Ghosh, 2014). It binds a C-terminal motif of Hsp70 and Hsp90 chaperone family proteins and targets misfolded client proteins of these chaperones for proteasomal degradation (Paul and Ghosh, 2014). Interestingly, a recent study showed that caspase cleavage can lead to the exposure of a degron sequence recognized by CHIP at the novel C-terminus of the client protein (Ravalin et al., 2019).

Here we identify a previously unknown cleavage site at D65 of Tau, which is efficiently processed by caspase-2, and we further show that this enzyme can also cleave Tau at D421. This results in the truncation of Tau at both the N- and C-termini, generating a fragment with strong aggregation propensity *in vitro*. In addition, we find that CHIP-mediated ubiquitination of Tau is strongly induced after caspase-2 cleavage, and Tau fragments show significantly accelerated clearance compared to the full-length protein in cultured cells. The truncated proteins also exhibit preferential binding to CHIP and a strong reduction of steady-state levels compared to full-length Tau after overexpression in mouse hippocampal tissue. Our findings thus suggest that CHIP-mediated degradation may prevent the accumulation of caspase-2 generated Tau fragments *in vivo*.

2. Materials and methods

2.1. Recombinant Tau purification

Full-length Tau 1N4R, 2N4R and Tau fragments 1–421 (2N4R) and 66–421 (2N4R) were expressed and purified as described previously (Behrendt et al., 2019). Briefly, *E. coli* BL21(DE3) cells (Sigma, cat. no. CMC0014) transformed with a pET19 vector containing the Tau construct were induced by the addition of 1 mM IPTG and harvested by centrifugation. Cleared lysates in 50 mM Na-phosphate pH 7.0, 1 mM EGTA, 1 mM DTT, cOmplete protease inhibitors (Roche), benzonase (Merck) and 10 μg/ml lysozyme (Sigma) were boiled for 20 min at 100 °C. Supernatants were loaded onto a combination of a HiTrap Q and a HiTrap SP column (GE Healthcare) and eluted in a gradient to running buffer containing 300 mM NaCl. Tau-containing fractions were further purified with a HiLoad 16/600 Superdex 75 pg size exclusion chromatography column (GE Healthcare). Fractions were analyzed by SDS-PAGE, pooled according to purity, flash-frozen in liquid nitrogen and stored at −80 °C.

2.2. Thioflavin T assay

10 μM recombinant Tau protein (in 20 mM Tris pH 7.5 containing 100 mM NaCl, 1 mM EDTA, 1 mM DTT) were mixed with 0.03 mg/ml heparin sodium salt (Sigma Aldrich) and 30 μM thioflavin T (Sigma Aldrich) and incubated at 37 °C in a black 96 well plate in a FLUOstar optima plate reader (BMG Labtech). Fluorescent signals were measured every 30 min for a time frame of 60 h using 450 nm for excitation and 520 nm for emission as described previously (Behrendt et al., 2019).

2.3. In vitro caspase digest

3 μg full-length recombinant Tau 1N4R protein were incubated with human caspases 1–10 (Enzo Life sciences) a final concentration of 10 U/μl for 1 h at 37 °C in caspase cleavage buffer (100 mM HEPES pH 7.4, 200 mM NaCl, 0.2% CHAPS, 2 mM EDTA, 20% glycerol, 10 mM DTT). Samples were subsequently analyzed by SDS-PAGE as described below.

2.4. Human brain samples

Anonymized human post-mortem tissue was obtained from the London Neurodegenerative Diseases Brain Bank and the Southwest Dementia Brain Bank, members of the Brains for Dementia Research Network. Tissue donor characteristics are summarized in Suppl. Table S1.

2.5. Acid hydrolysis for mass spectrometric determination of N- and C-termini in caspase-cleaved recombinant Tau

Samples were separated on a 10% Tris-Tricine SDS-PAGE gel (Thermo). Excised bands from recombinant 2N4R Tau with/without caspase-2 digest (band 1 and band 2, respectively) were transferred into tubes and shrunk with 100% ACN for 15 min at room temperature. Gel pieces were treated with 10 mM Dithiothreitol (DTT) followed by another shrinkage procedure. This was repeated with 55 mM Iodoacetamide (IAA). For determination of the protein sequence (Myrum et al., 2015), gel pieces were dried and transferred to glass vials (Chromacol) and covered with 3 M HCl. After 5 min incubation, tubes were put in a microwave set to 100% power and 10 min. Supernatant was desalted using C18 cartridges (OASIS, Waters) and analyzed on LC-MS as described (Myrum et al., 2015). In brief, peptides were separated using the nanoAcquity UPLC system (Waters) fitted with a trapping (nanoAcquity Symmetry C18, 5 μm, 180 μm × 20 mm) and analytical column (nanoAcquity BEH C18, 1.7 μm, 75 μm × 200 mm) coupled directly to a linear trap quadropole (LTQ) Orbitrap Velos (Thermo Fisher Scientific) with a Proxeon nanospray source. Solvent A was water+0.1% formic acid and solvent B was acetonitrile+0.1% formic acid. Samples were loaded with a constant flow of solvent A at 5 μl/min on to the trapping column. Peptides were eluted *via* the analytical column at a constant flow of 0.3 μl/min. The peptides were introduced into the mass spectrometer (Orbitrap Velos Pro, Thermo) *via* a Pico-Tip Emitter 360 μm OD (outer diameter) × 20 μm ID (inner diameter); 10 μm tip (New Objective) and a spray of 2.2 kV was applied. Full scan MS spectra with mass ranges of 300–1700 m/z were acquired in the fourier transform (FT) profile mode with resolution of 30,000. The most intense ions (up to 15) from the full scan MS were selected for sequencing. Data processing was performed using isobarQuant software (Franken et al., 2015) and MASCOT (Matrix Science). The data were searched against a *Homo sapiens* Uniprot database including the specific sequence of Tau—F. The data were searched with the following modifications: fixed carbamidomethylation on cysteine and variable oxidation on methionine. Only rank 1 peptides with a minimum Mascot score of 15 were used for sequence coverage, peptides identified are summarized in Suppl. Table S2.

2.6. LC-MS/MS of Tau immunopurified from human brain samples

The detailed sample preparation and MS workflow is described elsewhere (Behrendt et al., 2019). In brief, human entorhinal cortex was homogenized in Triton lysis buffer (50 mM NaCl; 20 mM Tris, pH 7.5; 1 mM EDTA; 1 mM EGTA; 1% Triton-X-100; 1× Protease inhibitors; 1× Phosphatase inhibitors (both Roche), 500 μM IOX1, 2 μM Daminozide, 10 μM Trichostatin A, 5 mM Nicotinamide, 10 μM Paragyline hydrochloride, 1 μM Thiamet G), and Tau was immunoprecipitated using a combination of total Tau antibodies (Tau-12, Biolegend; Tau-5, Abcam; HT7, Thermo Fisher). Samples were separated by SDS-PAGE, stained with Coomassie Staining solution (0.1% Coomassie Blue G250, 1 M ammonium sulfate, 30% methanol, 3% o-phosphoric acid) and bands excised. Samples were subjected to either an in-gel tryptic- or to an in-gel AspN digest and peptides were analyzed using nanoAcquity UPLC (Waters) with a nanoAcquity trapping (nanoAcquity Symmetry C18, 5 μm, 180 μm × 20 mm) and analytical column (nanoAcquity BEH C18, 1.7 μm, 75 μm × 200 mm), which was coupled to an LTQ Orbitrap Velos Pro (Thermo Fisher) using the Proxeon nanospray source. For data analysis, only peptides corresponding to semi-trypsin or semi-AspN digests were considered.

2.7. Intracellular Tau ubiquitination, cleavage, and degradation analyses

For intracellular Tau cleavage analyses, HEK293 cells were seeded at 3.5×10^5 cells/well into six-well dishes and co-transfected the next day with pCDNA3_HA-Tau 2N4R-1-441 (WT, D65E, D421E or D314E) and

pCMV6-Entry_caspase-2-myc-DDK using Lipofectamine 3000 (Invitrogen) according to manufacturer's instructions. For reference samples, single transfections of pCDNA3_HA-Tau 2N4R-1-441, pCDNA3_HA-Tau 2N4R-1-421, pCDNA3_HA-Tau 2N4R-66-421, pCDNA3_HA-Tau 2N4R-66-441 or pCDNA3_HA-Tau 2N4R-1-314 were performed. Cells were scraped off the plate 24 h later, pelleted and washed with ice-cold 1× PBS (Gibco). Pellets were stored at −80 °C until lysis.

For Tau ubiquitination and degradation analyses, HEK293 cells were transfected with full-length tau or tau fragments, CHIP E3 ligase and ubiquitin. In brief, 3.5×10^5 HEK293 cells per well were seeded in a six-well dish (Thermo Scientific). Subsequently, cells were co-transfected using Lipofectamine 3000 (Invitrogen) according to manufacturer's instruction with the following plasmids: Either 1 μg pCDNA3_HA-Tau 2N4R-1-441, or 1 μg pCDNA3_HA-Tau 2N4R-1-421, or 1 μg pCDNA3_HA-Tau 2N4R-66-421 were co-transfected with 1 μg pReceiver-M12_3xFlag-hUBB and 0.5 μg NanoBRET-CHIP plasmid. As a control, 1 μg 3xFlag-hUBB, 0.5 μg NanoBRET-CHIP and 1 μg pReceiver-M98-meGFP plasmid were co-transfected. For protein degradation analyses, cells were treated with 200 μg/ml Cycloheximide (Sigma-Aldrich) for 3 h and 6 h the next day or left untreated. Samples were collected in 1 ml ice-cold 1× PBS (Gibco), centrifuged at 300 ×*g* for 10 min and pellets were stored at −80 °C.

2.8. Cell and tissue lysis, SDS-PAGE and Western blotting

Cell pellets were lysed in 100 μl lysis buffer (150 mM NaCl, 20 mM Tris pH 7.5, 1 mM EDTA, 1 mM EGTA, 1% Triton-X100) supplemented with cOmplete Protease inhibitor and PhosSTOP phosphatase inhibitor cocktails (both Roche) for 10 min on ice followed by 10 min centrifugation at 12.000 ×*g* and 4 °C. Protein concentrations in the supernatants were measured using the BCA protein assay (BioRad). Aliquots corresponding to 50 μg total protein were mixed with Lämmli sample buffer, denatured for 10 min at 95 °C and separated by SDS-PAGE as described below.

Mouse hippocampus samples were homogenized in Triton lysis buffer (150 mM NaCl, 20 mM Tris pH 7.5, 1 mM EDTA, 1 mM EGTA, 1% Triton-X100 and protease, phosphatase, demethylase (500 μM IOX1, 2 μM Daminozide, 10 μM Paragyline Hydrochloride), deacetylase (10 μM Trichostatin A, 5 mM Nicotinamide), O-GlcNAcase (1 μM Thiamet-G) inhibitors) with a Dounce homogenizer (Carl Roth). The tubes were twice scraped over a hard surface with in-between incubation on ice for 10 min. Samples were centrifuged for 20 min at 16000 ×*g* at 4 °C, the protein concentration in the supernatant was determined with a BCA assay (BioRad, cat. No. 5000112) and 25 μg total protein were boiled at 95 °C for 5 min in sample buffer for SDS-PAGE.

Samples were separated using pre-cast 12% gels with MES running buffer (caspase-2) or 10% gels with MOPS running buffer (Tau; all gels from the Bio-Rad Criterion system). Gels were immunoblotted onto PVDF membranes (Merck Millipore) using a semi-dry transfer apparatus (Bio-Rad Trans-Blot SD). Membranes were blocked in Odyssey blocking buffer (TBS, Li-Cor Biosciences) for 30 min at room temperature and incubated with primary antibodies over night at 4 °C: Tau12, mouse, 1:500, (Biolegend, cat. no. 806501); HT7, mouse, 1:500, (Thermo Fisher, cat. no. MN1000); Tau-5, mouse, 1:1000, (Abcam, cat. no. ab80579); DAKO-Tau, 1:5000–1:10000, (Dako/Agilent, cat. no. A0024); Tau—C3, rabbit, 1:1000, (Sigma Aldrich, cat. no. 36–017); GAPDH, 1:5000, (Cell Signaling Technology, cat. no. 2118); actin, mouse, 1:1000–1:5000, (Sigma Aldrich, cat. no. A5441); DDK/Flag, 1:2000, (Sigma Aldrich, cat. no. F3165); Antibodies were diluted in 5% BSA in 1× TBST (1× TBS, 0.05% Tween-20). The next day, membranes were washed three times with 1× TBST, and secondary antibody incubations (1:20000, IRDye Donkey anti-mouse/rabbit 800 and IRDye Donkey anti-mouse/rabbit 680) were done in blocking solution for one hour at RT. The membranes were then washed three times with 1× TBST, once with 1× TBS and imaged on a Li-Cor Odyssey CLx scanner.

2.9. Cell lysis and ELISA

Transfected HEK T293 cells were lysed in 200 μl lysis buffer (150 mM NaCl, 20 mM Tris pH 7.5, 1 mM EDTA, 1 mM EGTA, 1% Triton-X100) supplemented with cOmplete Protease inhibitor and PhosSTOP phosphatase inhibitor cocktails (both Roche) for 10 min on ice followed by 10 min centrifugation at 12.000 ×*g* and 4 °C. Total Tau as well as ubiquitinylated Tau was determined using the V-PLEX Human Total Tau Kit (K151LAE, Meso Scale Discovery). For total Tau analysis, samples were diluted 1:900 and total Tau levels were determined following the manufacturer's instructions. For ubiquitinylated Tau analysis, samples were diluted 1:300 and ubiquitinylated Tau was detected using the plate from the V-PLEX Human Total Tau Kit (K151LAE, Meso Scale Discovery) for capture of Tau, and an anti-ubiquitinylated Protein SULFO-TAG labeled antibody (R32AU, Meso Scale Discovery) at a final concentration of 0.5 μg/ml for detection. Samples from cells without Tau transfection were used as negative controls. Plates were measured on a Meso Scale Quickplex platform.

2.10. In vitro ubiquitination assays

For *in vitro* ubiquitination assays, recombinant proteins and reagents were purchased from Boston Biochem (CHIP Ubiquitin Ligase Kit - Glow-Fold Substrate, Cat. # K-280). *In vitro* reactions were carried out according to the manufacturer's instructions. Full-length Tau 2N4R was obtained from Boston Biochem (Tau 441 (2N4R), human recombinant cat. # SP-495), Tau fragments 1–421 and 66–421 were expressed as described above and a final concentration of 0.164 μM was used in the *in vitro* reactions. A total volume of 30 μl containing E1, E2, E3 enzyme, reaction buffer, Mg^{2+}-ATP solution, HSP70/HSP40 Mix, and Tau substrate (according to Boston Biochem's protocol) were used. Reactions were initiated by the addition of ubiquitin and incubated in a water bath at 37 °C. At indicated timepoints (0, 15, 30, 45, 60 and 90 min) an aliquot (5 μl) was removed, and the reaction was terminated by adding 5 x SDS PAGE sample buffer supplemented with 100 mM DTT and boiling for 5 min at 95 °C. Samples were analyzed by SDS-PAGE on a 4–20% gradient precast gel (Bio-Rad, Criterion) followed by immunoblotting onto PVDF membranes using the Bio-Rad Trans-Blot Turbo Transfer System. Membranes were blocked with 5% milk in TBST (50 mM Tris-HCl (pH 7.6), 150 mM NaCl, 0.05% Tween 20). Blots were incubated overnight at 4 °C with primary Tau-antibody (Anti-Tau, Abcam cat. #64193, 1:2000). Blots were washed three times (each 5 min) with TBST and incubated for 1 h at room temperature with secondary antibodies (HRP-conjugated for chemiluminescence, anti-rabbit, Dianova/Jackson ImmunoResearch, cat. # 111–035-144, 1:10000). Blots were washed three times with TBST. For chemiluminescence visualization, blots were incubated with Western blotting detection reagent (SuperSignal West Pico PLUS Chemiluminescent Substrate, ThermoFisher) and detected with a ChemiDoc Touch Imaging System (Bio-Rad).

2.11. Mouse model

Homozygous female and male MAPT knockout mice (strain #007251, Jackson Laboratories) were used in the study (Dawson et al., 2001). All transgenic mice were obtained by and bred at the DZNE (Bonn, Germany). Mice were group-housed in colonies of up to five mice, separated by sex in individually ventilated cages under specific-pathogen-free conditions with unlimited access to food and water. The tap water was preprocessed in three steps to reduce the risk of bacterial and fungal growth: microfiltration, ultraviolet decontamination, and mild acidification to pH 5.5. The light and dark cycle was 12 h/12 h and the temperature was kept constant at 22 °C. Equal numbers of male and female mice were randomly assigned to the experimental groups. Behavioral experiments were carried out during the light cycle. All procedures were performed in accordance with an animal protocol approved by the DZNE and the government of North-Rhine-Westphalia.

At 10 months of age, mice were anesthetized with a double dose of ketamine/xylazine (0.26/0.02 mg/kg bodyweight) until surgical tolerance was reached. Subsequently, mice were transcardially perfused with PBS pH 7.4, brains were removed, and the two hemispheres were separated along the midline. Immediately, from one hemisphere, the hippocampus was dissected in ice-cold PBS pH 7.4, snap-frozen in liquid nitrogen and stored at −80 °C until further use. The other hemisphere was placed into 4% paraformaldehyde in PBS (PFA) for 24 h, and subsequently transferred to 1× PBS with 0.01% sodium azide for subsequent immunohistochemical analyses.

2.12. AAV injection

Littermate mice were randomized and bilaterally injected with AAV-hSyn-Tau-1-441, AAV-hSyn-Tau-1-421, AAV-hSyn-Tau-66-421 or AAV-hSyn-tdTomato-WPRE (Addgene #51506). The constructs containing the three different Tau-fragments (Tau-1-441, Tau-1-421, Tau-66-421) were cloned into the pAAVSyn1-tdTomato vector (Addgene #104060) by replacing the tdTomato sequence and adding a WPRE element. Bilateral injections were delivered to the dorsal CA1 region of the hippocampus at two months of age. To this end, mice were anesthetized with ketamine/xylazine (0.13/0.01 mg/kg bodyweight) and transferred to a stereotactic frame upon surgical tolerance. A small incision was made along the midline to expose the bregma. Small holes were drilled at −1.95 mm (AP), ±1.50 mm (ML) starting from bregma. The stereotactic frame was equipped with a micromanipulator (Luigs&Neumann) to carry a Hamilton syringe with a 27 G needle. The Hamilton syringe was connected to a micropump that was used to inject a volume of 0.7 µl virus at 0.1 µl/min per hemisphere at a depth of 1.15 mm (DV) from brain surface. After injecting the virus, the needle was left at the site of injection for 5 min to allow the virus to diffuse into the tissue before the needle was removed and the skin was closed with stitches. Mice received temgesic analgesia (0.5 mg/kg bodyweight) every 6–8 h for a period of up to three days.

2.13. Immunohistochemical procedures

Embedding, cutting and immunofluorescent staining of mouse brains was performed by Morphisto GmbH (Offenbach, Germany). Briefly, PFA- fixed brain hemispheres dehydrated in ethanol, infiltrated with xylol and paraffin at 58 °C and embedded in paraffin. Blocks were sectioned sagitally on a microtome, and 5 µm sections were mounted on slides. For immunohistochemistry, samples were deparaffinated with xylol, hydrated with ethanol and subjected to epitope retrieval with 10 mM citrate buffer pH 6 (Morphisto) with 3 × 5 min cycles at 800 W in a microwave. Slides were washed with PBS and endogenous peroxidase was quenched with 0.6% H_2O_2 followed by another wash step in PBS and blocking with normal horse serum (ImmPress Kit, Vectorlabs).

For NeuN histochemistry, an overnight incubation with primary antibody (NeuN, MAB377, Merck Millipore; 1:1000 dilution) in PBS with 2% normal horse serum and 1% BSA was performed at 4 °C. Slides were then washed in PBS, incubated for 30 min at room temperature with secondary antibody (anti-mouse ImmPress HRP reagent, ImmPress Kit, Vectorlabs), followed by washes with PBS and 50 mM Tris/HCl pH 7.6. Slides were incubated for 5 min in DAB solution (50 mM Tris/HCl pH 7.6 with 0.01% H_2O_2 and 0.025% DAB (Sigma Aldrich)) at room temperature, washed with distilled water at 4 °C and counterstained with hematoxylin before the addition of CV mount medium (Leica Biosystems) and coverslips.

For immunofluorescent detection of Tau, slides were incubated for 15 min with primary antibody (HT7, MN1000, ThermoScientific; 1:1000 dilution) in PBS with 2% normal horse serum and 1% BSA at 4 °C. Slides were then washed in TBST (Morphisto), incubated for 10 min at room temperature with secondary antibody (anti-mouse ImmPress HRP reagent, ImmPress Kit, Vectorlabs), followed by washes with TBST. Next, slides were incubated for 10 min in Opal working solution (1:150 dilution, Opal 520 Reagent Pack, cat. no. FP1487001KT, Perkin Elmer) at room temperature in the dark to generate fluorescent signal for total Tau. Slides were then washed with TBST and subjected to microwave treatment in 10 mM citrate buffer pH 6 (Morphisto) for 1–3 min at 800 W (until boiling), followed by 15 min at 200 W. After cooling down, samples were washed in TBST and blocked for 10 min in normal horse serum at room temperature. The second incubation with primary antibody (AT8, MN1020, ThermoScientific; 1:150 dilution) was performed in PBS with 2% normal horse serum and 1% BSA for 15 min at room temperature.

Slides were then washed in TBST (Morphisto), incubated for 10 min at room temperature with secondary antibody (anti-mouse ImmPress HRP reagent, ImmPress Kit, Vectorlabs), followed by washes with TBST. Next, slides were incubated for 10 min in Opal working solution (1:150 dilution, Opal 650 Reagent Pack, cat. no. FP1496001KT, Perkin Elmer) at room temperature in the dark to generate fluorescent signal for phosphorylated Tau.

Samples were then washed in TBST and H_2O, counterstained with DAPI in PBS and mounted with Prolong GOLD antifade mounting medium (P36934, Invitrogen) and stored in the dark at room temperature. Negative controls were performed by omitting the primary antibody.

pT231-modified Tau was detected on 4 µm sections using a Leica Bond Rx system (Leica Biosystems) using the Leica Bond Polymer Refine Detection Kit according to manufacturer's instructions. The pT231 Tau antibody (cat. no. ab151559, Abcam) was used at a dilution of 1:30,000 in PBS with 1% donkey serum, and DAB-based detection was performed according to the kit instructions. CV Mount medium (Leica Biosystems) was used for mounting of slides.

For RNAScope analysis, formalin-fixed, paraffin-embedded sections were processed on the Leica Bond RX system (Leica Biosystems) using the RNAscope 2.5 LSx Kit (ACD, USA) according to the manufacturer's manual. A custom-made probe recognizing all Tau fragments used in the study was designed and generated by ACD and used for hybridization. In short, sections were baked and deparaffinized in the Bond RX, followed by target retrieval (15 min at 95 °C using Leica Epitope Retrieval Buffer 2) and protease treatment (15 min at 40 °C). The probes were then hybridized for 2 h at 42 °C followed by RNAscope amplification followed by Fast Red chromogenic detection.

For quantification of pT231 Tau and RNAScope staining, three hippocampal areas per animal were outlined and the covered area was quantified using the HALO software (Indica Labs).

2.14. Morris water maze

At 10 months of age, animals were tested for cognitive performance using the Morris water maze (MWM) (Morris, 1984; Vorhees and Williams, 2006). Researchers performing the test and analyzing the data were blinded to the experimental groups. Animals were placed into a circular pool of opaque water at 20 °C, with a submerged platform in the northeastern quadrant. Fixed visual cues were placed around the pool, and the researchers were visually shielded from the pool by walls. During the learning phase, animals were tested in four trials per day with an inter-trial interval of 30 min on five consecutive days with alternating starting quadrants and a maximal duration of 60 s per trial. On day 6 (trial day), the platform was removed, and mice were left to swim for 60 s. Trials were filmed with a ceiling camera and data analyzed using EthoVision XT13 software.

2.15. Immunoprecipitation

Mouse brain lysate corresponding to 30 µg total protein were diluted to 200 µl in Triton lysis buffer (150 mM NaCl, 20 mM Tris pH 7.5, 1 mM EDTA, 1 mM EGTA, 1% Triton-X100, 1× cOmplete Protease inhibitors (Roche), 1× PhosStop Phosphatase inhibitors (Roche)). 10 µl sample were removed and stored at −20 °C (input). For each sample, 20 µl anti-mouse Dynabeads (Invitrogen) were washed 3× with 200 µl PBS + 0.1%

BSA, followed by 30 min of incubation on a shaker at room temperature with 1 µg HT7 antibody (Thermo Fisher) in a total volume of 200 µl PBS + 0.1% BSA. The beads were washed once with 200 µl Triton lysis buffer and mixed with the brain lysate. Samples were incubated over night at 4 °C on a shaker, 10 µl post-immunoprecipitation supernatant was collected and the beads were washed twice with Triton lysis buffer. 10 µl Lämmli buffer was added, and all samples were denatured at 98 °C for 10 min with subsequent separation on 4–20% gradient gels (Bio-Rad Criterion) followed by immunoblotting onto PVDF membranes using the Bio-Rad Trans-Blot Turbo Transfer System. Membranes were blocked for 30 min at room temperature using fluorescent blot blocking buffer (Azure Biosystems) and incubated with primary antibodies over night at 4 °C: DAKO-Tau, rabbit, 1:10000, (Dako/Agilent, cat. no. A0024); STUB/CHIP, rabbit, 1:2000 (Abcam, cat. no. ab134064). Antibodies were diluted fluorescent blot blocking buffer (Azure Biosystems). The next day, membranes were washed three times with 1× fluorescent blot washing buffer (Azure Biosystems), and secondary antibody incubations (1:10000, Azure Spectra 700 goat-anti-rabbit IgG, Azure Biosystems) were done in blocking solution for one hour at RT. The membranes were then washed three times with 1× fluorescent blot washing buffer (Azure Biosystems) and imaged on a ChemiDoc Touch Imaging System (Bio-Rad).

2.16. Data analysis

Immunoblotting data were analyzed using Image Studio Lite (Li-cor Biosciences) and statistical analysis was performed with GraphPad Prism 7 (GraphPad Software) using the test noted within the respective figure legend.

3. Results

3.1. Caspase-2 cleaves Tau at D65 and D421

To gain an unbiased overview of the cleavage pattern of Tau generated by members of the caspase family, we first subjected recombinant Tau protein to an *in vitro* enzymatic digest using all ten human caspases. As expected, we observed significant cleavage of Tau with caspases −3 and − 7, generating fragments truncated at D421 that can be detected with the respective neoepitope antibody Tau-C3 (Fig. 1A). Surprisingly we found that also caspase-2 was able to cleave Tau at D421, and this digest generated two additional cleavage fragments of approximately 40 kDa. The smaller of these fragments was also detected with the antibody Tau-C3 and therefore likely terminates in D421 (Fig. 1A, red arrow).

To further map the caspase-2 cleavage sites in Tau, we next performed biochemical analyses with N- and C-terminal Tau antibodies as well as mass spectrometry. Upon caspase-2 digest, both Tau 1N4R and 2N4R isoforms generated fragments with N-terminal truncation, since cleavage bands of 37–50 kDa in size were only detected with the C-terminal antibody DAKO-Tau, but not the N-terminal antibody Tau-12 (Fig. 1B). Bands corresponding to full-length and caspase-2 cleaved Tau were furthermore excised from a Coomassie-stained gel (Suppl. Fig. S1) for mass spectrometry analysis. Here we found that an N-terminal peptide ranging from amino acids (aa) 2–23 was clearly detected in the full-length Tau control, but completely absent from the cleaved sample. Additionally, while the non-cleaved control contained an aa 61–87 peptide, this was truncated to aa 66–87 specifically in the caspase-2 cleaved sample (Suppl. Fig. 1, Suppl. Table S2). These data thus indicate that Tau is cleaved by caspase-2 at aa 65, corresponding to the cleavage motif SETSD. Using CaspDB, an *in silico* cleavage site prediction tool for caspases (Kumar et al., 2014), we confirmed that this site may be a caspase recognition site. In fact, when the sequence of the longest isoform of Tau expressed in the CNS (2N4R) is taken into account, D65 is the second most likely caspase cleavage site after D421, with a probability score of 0.953 (Kumar et al., 2014).

We next investigated whether intracellular processing of Tau by caspase-2 follows the same pattern. To this end, we co-transfected Tau 2N4R with the pro-form of caspase-2 into HEK293 cells. The overexpression of caspase-2 thereby leads to its activation, as it promotes the formation of active dimers followed by auto-proteolysis to generate the active subunits (Baliga et al., 2004). Again, caspase-2 generated Tau fragments were only detected with the C-terminal DAKO-Tau, but not the N-terminal Tau-12 antibody, and cleavage is prevented when a D65E mutation is introduced (Fig. 1C). The D65E mutant Tau co-expressed with caspase-2 furthermore exhibits an additional band on the Tau-12 blot (Fig. 1C, black arrow), which runs slightly below the non-cleaved protein and may represent the Tau 1–421 fragment. Consistent with this observation, we observed a slight upwards shift of the D421E cleavage band on the DAKO-Tau blot (Fig. 1C, red arrow), indicating that the ~50 kDa cleavage fragment is truncated at both D65 and D421 in WT Tau. We furthermore show that cleavage in our system does not involve the previously described site at D314 (Zhao et al., 2016), since a D314E mutant Tau construct did not abolish fragment generation (Fig. 1C). Taken together, we thus confirmed that caspase-2 cleaves Tau at D65 *in vitro* and in mammalian cells and is furthermore capable of processing the well-described caspase site at D421.

3.2. Caspase-2 derived Tau fragments are aggregation-prone and present in human brain tissue

Tau fragments are known to aggregate more readily than the full-length protein, and proteolytic cleavage has been associated with the formation of NFTs in AD (Quinn et al., 2018; Wang and Mandelkow, 2016). To determine whether the fragments generated by caspase-2 are more aggregation prone than the full-length protein, we next analyzed the aggregation potential of the different Tau proteins *in vitro*. Using the amyloid fibril-binding dye Thioflavin T as a readout, we found that the double truncation of Tau at both the N- and C-termini accelerated the aggregation of the protein, with the first signal increase becoming apparent at the 6 h timepoint (Fig. 1D). Tau 1–421 only led to a signal increase starting at approximately 50 h of incubation, and the slope of the signal increase was dramatically reduced compared to Tau 66–421. The full-length Tau protein only led to very little Thioflavin T fluorescence signal under these conditions after app. 60 h of incubation (Fig. 1D).

To determine whether caspase-2 derived Tau fragments may be present in human brain tissue, we next re-analyzed mass spectrometry data of Tau immunopurified from human control and AD patient entorhinal cortex samples (Behrendt et al., 2019). In a control brain sample we identified both semi-tryptic and semi-AspN peptides initiating at aa66, suggesting that Tau cleavage at D65 had occurred (Table 1). The same semi-tryptic and semi-AspN peptides were identified in an AD patient brain from the same data set, however the confidence threshold for detection (Mascot score > 20) was not met in this second sample. Furthermore, and consistent with published reports (Basurto-Islas et al., 2008; Behrendt et al., 2019; Guillozet-Bongaarts et al., 2005; Nicholls et al., 2017), peptides truncated at D421 were also present in our dataset in both control and AD patient brains (Table 1). Taken together these data thus indicate that Tau is cleaved at D65 in human brain tissue, in addition to the previously reported D421 cleavage.

3.3. Tau fragments exhibit low steady-state protein levels in vivo

To further investigate the effects of caspase-2-derived Tau fragments *in vivo*, we next expressed full-length human 2N4R Tau as well as Tau fragments in the hippocampus of MAPT ko mice using stereotactic injections of AAV constructs at two months of age. A group of mice with AAV-mediated expression of tdTomato was used as a control. Mice were then subjected to behavioral analyses at twelve months of age, 10 months after the hippocampal injection of AAV, and brain tissues were harvested for further analyses.

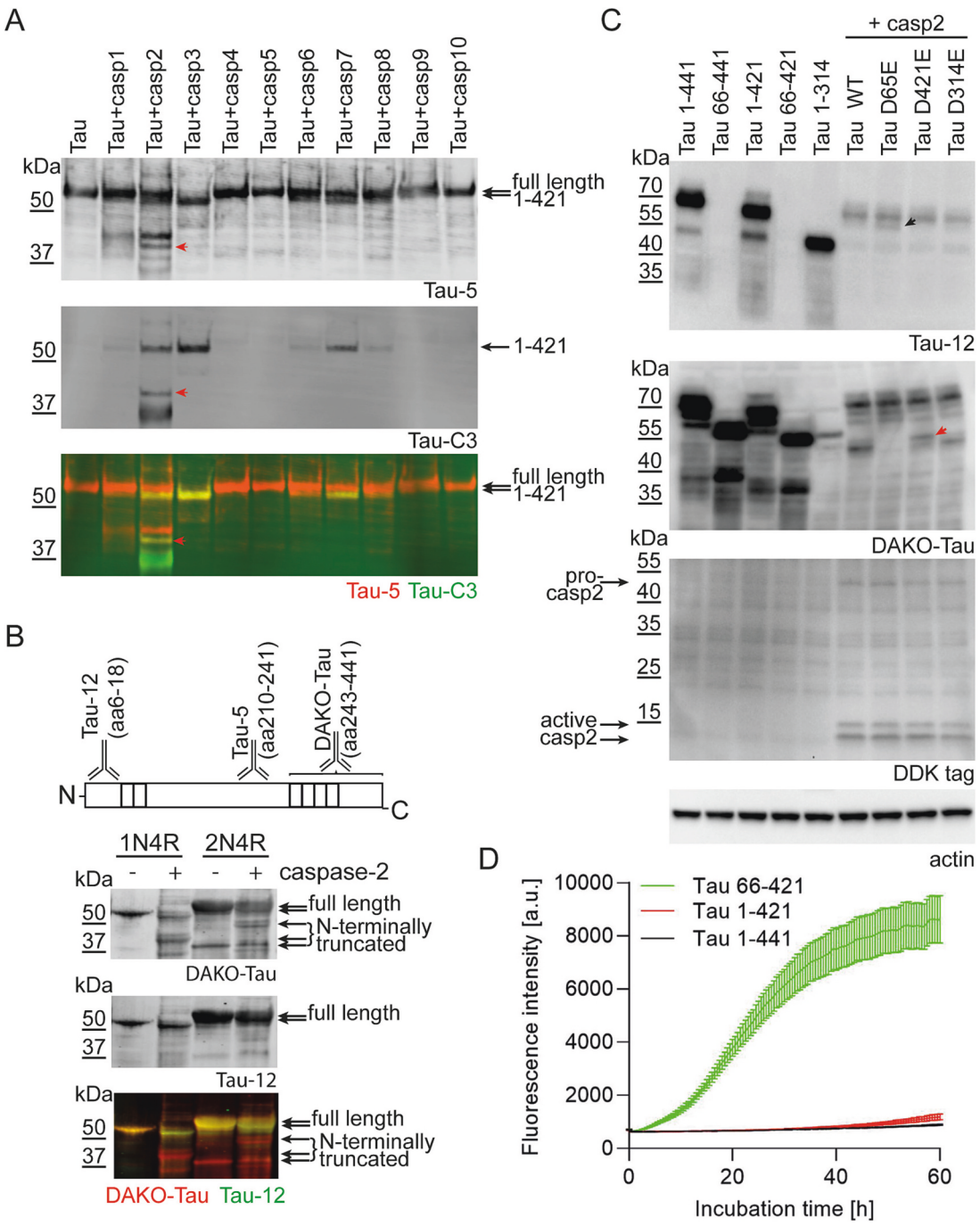

Fig. 1. Caspase-2 cleaves Tau at D421 and D65, generating an aggregation-prone fragment.
(A) Recombinant Tau 1N4R protein was subjected to digests with each of the 10 human caspase enzymes *in vitro*. Western blot analyses using the total Tau antibody Tau-5 as well as the D421 neoepitope antibody Tau-C3 demonstrate that caspases −2, 3, 6, 7 and 8 can cleave Tau at D421. Caspase-2 cleavage further generates bands of approximately 40 kDa, one of which (red arrow) is recognized by both Tau-5 and Tau-C3 and should thus correspond to a Tau fragment terminating in D421. (B) Caspase-2 cleavage of both recombinant 1N4R and 2N4R Tau proteins generates fragments lacking the Tau N-terminus, which do not react with antibody Tau-12. (C) Co-transfection of 2N4R Tau and DDK-tagged caspase-2 in HEK293 cells generates fragments lacking the Tau N-terminus. Generation of the ~50 kDa fragment is prevented in D65E mutant Tau, accompanied by the appearance of a larger Tau-12 reactive band that may represent Tau 1–421 (black arrow). Cleavage of D421E Tau generates a slightly larger fragment detected by DAKO-Tau, likely representing Tau 66–441 (red arrow). No changes in Tau cleavage are observed upon co-expression of Tau D314E with caspase-2. The overexpression of caspase-2 leads to its autoactivation as demonstrated by the presence of active caspase-2 subunits in transfected samples. (D) The recombinant Tau 66–421 fragment shows strongly accelerated aggregation with a significantly shorter lag time compared to Tau 1–421 or full-length Tau. Tau aggregation was monitored using fluorescence of the amyloid fibril-reactive dye Thioflavin T as a readout. Representative graphs and images of $n = 3$ independent experiments are shown.

Table 1
List of peptides truncated at D65 or D421 identified by mass spectrometry on Tau immunopurified from control or AD patient human brain samples. Peptide sequences are numbered corresponding to the longest Tau isoform (Tau 2N4R, 441 aa). | indicates the junction of exon 2 to exon 4, indicating the peptide is derived from a 1 N isoform.

Sample ID	aa- residues	peptide	digestion enzyme	MW (Da)	Error (p.p.m.)	Mascot score
Ctrl 3	66–115	AKSTPTAE|AEEAGIGDTPSLE	AspN	2072.97494	1.3	49
Ctrl 3	66–126	AKSTPTAE|AEEAGIGDTPSLEDEAAGHVTQAR	Trypsin	3208.51198	-1.01	55
Ctrl 1	407–421	HLSNVSSTGSIDMVD	Trypsin	1576.70391999999	0.49	51
Ctrl 2	402–421	DTSPRHLSNVSSTGSIDMVD	AspN	2132.96445	1.63	24
Ctrl 2	407–421	HLSNVSSTGSIDMVD	Trypsin	1576.70391999999	0.41	62
Ctrl 3	407–421	HLSNVSSTGSIDMVD	Trypsin	1576.70391999999	-2.61	36
Ctrl 3	407–421	HLSNVSSTGSIDMVD	Trypsin	1576.70391999999	-0.75	54
AD 1	402–421	DTSPRHLSNVSSTGSIDMVD	AspN	2132.96445	2.83	34
AD 1	407–421	HLSNVSSTGSIDMVD	Trypsin	1576.70391999999	1.03	63
AD 3	407–421	HLSNVSSTGSIDMVD	Trypsin	1576.70391999999	-0.21	52

First, we used the Morris water maze (MWM) test to assess spatial learning and memory. Over a period of five days, mice were trained to locate a hidden platform in the northeastern quadrant of the maze. During this training period, no significant differences between groups were observed, and all animals learned to quickly navigate to the platform at the end of day five (Fig. 2A). The next day, the platform was removed and the time the animals spent in the different quadrants of the maze was scored. Mice expressing Tau 1–421 or Tau 66–421 fragments thereby behaved similar to the tdTomato expressing control group and spent similar amounts of time in the area that previously contained the platform compared to the other areas of the maze (Fig. 2B). For mice expressing full-length Tau 1–441, however, a significant reduction in the time spent in the platform area was observed compared to the other three experimental groups (Fig. 2B). These data indicate that the presence of Tau fragments alone is not sufficient to induce cognitive deficits in our mouse model, while the overexpression of full-length Tau leads to impaired performance in the MWM test.

To quantify transgene expression, we determined hippocampal Tau protein levels by Western blotting. We found that full-length Tau protein was expressed at significantly higher levels than both Tau 1–421 and Tau 66–421 (Fig. 3A), with some mice exhibiting barely detectable levels of Tau 66–421. In contrast, *in situ* hybridization analysis with a custom probe designed to detect all Tau fragments showed strong expression of all Tau constructs at the RNA level (Fig. 3B), suggesting that the decrease observed for Tau 1–421 and Tau 66–421 protein is likely post-transcriptional.

Tau is subject to many PTMs, and hyperphosphorylation in particular is a hallmark of Tau-associated pathology (Ercan-Herbst et al., 2019; Wang and Mandelkow, 2016; Wesseling et al., 2020). Using Western blotting to assess the phosphorylation of Tau or Tau fragments *in vivo* we found that the relative phosphorylation of Tau 1–421 and Tau 66–421 at T181 is significantly reduced (Fig. 4A), while T231 phosphorylation is increased on both Tau fragments compared to full-length Tau 1–441 (Fig. 4B). However, due to the strong reduction of total Tau in mice expressing Tau fragments, this does not translate into an accumulation of phospho-Tau: Absolute levels of pT231 Tau (normalized to GAPDH levels) in mice expressing Tau fragments do not significantly exceed those in Tau 1–441 expressing animals (Fig. 4C).

We further complemented our analyses of Tau and phospho-Tau levels in the hippocampus of Tau-AAV-injected mice by immunohistochemistry. In agreement with Western blot data, we found the highest levels of human Tau protein (detected with antibody HT7) in animals expressing Tau 1–441 (Fig. 5A). Tau 1–421 protein was present at intermediate levels, while only very few cells in the CA2 hippocampal area were immunoreactive for HT7 in mice expressing Tau 66–421 (Fig. 5A). The CA2 region was also the area with the strongest HT7 signal in Tau 1–441 and Tau 1–421 expressing mice, suggesting that Tau levels in general were highest in this brain area in our model. The phospho-Tau antibody AT8, which recognizes an epitope associated with AD pathology (pS202/pT205), only showed minimal immunoreactivity in mice expressing full-length Tau or Tau fragments (Fig. 5A). In agreement with Western blot data, we observed strong immunoreactivity with a pT231 Tau antibody in all three groups of mice expressing full-length Tau or Tau fragments (Fig. 5B). As expected, mice expressing the tdTomato alone did not show any pT231 Tau immunoreactivity. Quantification of the NeuN immunoreactive hippocampal area showed no difference between the experimental groups (Fig. 5C), excluding the possibility that neuronal loss may influence the Tau and phospho-Tau quantification.

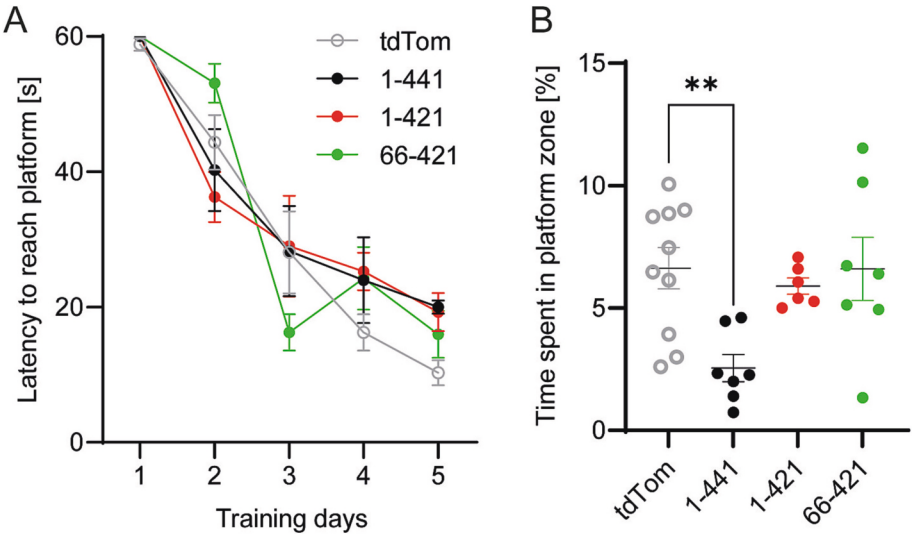

Fig. 2. Mice expressing caspase-2 derived Tau fragments do not exhibit cognitive deficits.
(A) No significant learning deficits were identified in mice overexpressing full-length Tau or Tau fragments in the MWM training period. (B) Mice expressing full-length Tau, but not Tau fragments, performed worse in remembering the location of the platform area on the test day in the MWM. No deficits were observed for mice expressing Tau fragments compared to the tdTomato control group. Statistical significance was determined by one-way ANOVA ($p < 0.01$), with Holm-Sidak's post-hoc comparisons test (**: $p < 0.01$), $n = 6$–10 animals per group.

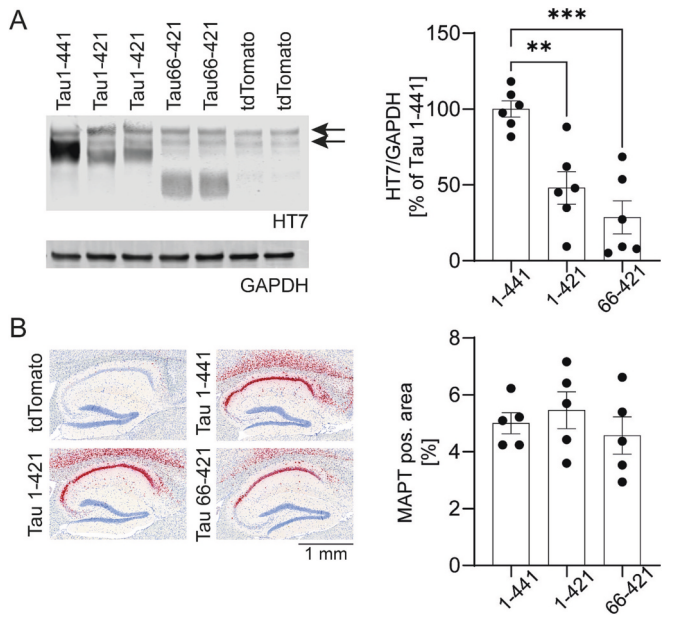

Fig. 3. Tau fragments exhibit lower steady-state protein levels *in vivo* compared to full-length Tau.
(A) Western blot analysis of hippocampal lysates demonstrates significantly lower Tau protein levels in mice expressing Tau 1–421 and Tau 66–421 compared to full-length Tau. n = 6 animals per group. Arrows indicate non-specific bands detected with HT7 antibody in all mice, including the tdTomato control group. (B) *In situ* hybridization demonstrates strong RNA expression levels for all three Tau constructs. $n = 5$ animals per group. Statistical significance was determined by one-way ANOVA: (A): $p < 0.001$; (B): $p = 0.5655$), with Tukey's post-hoc comparisons test (***: p < 0.001; **: $p < 0.01$).

Taken together, the data thus suggest that phosphorylation patterns are altered in mice expressing caspase-2 derived Tau fragments, however we do not observe an accumulation of phospho-Tau species. Furthermore, the sustained presence of all Tau transcripts indicates that the protein levels of Tau fragments are likely reduced in a post-transcriptional manner compared to full-length Tau, precluding unequivocal assignment of functional effects of Tau fragments *in vivo*.

3.4. *Caspase-2 generated Tau fragments are preferentially degraded after CHIP-mediated ubiquitination*

Tau is known to interact with the ubiquitin E3 ligase CHIP (Dickey et al., 2006; Petrucelli et al., 2004), and the loss of CHIP is linked to an accumulation of Tau truncated at D421 (Dickey et al., 2006; Ravalin et al., 2019). To investigate potential mechanisms that may be responsible for the low levels of caspase-2 derived Tau fragments, we next analyzed CHIP-mediated ubiquitination and degradation *in vitro* using a ubiquitination assay with recombinant Tau fragments or full-length Tau protein as substrates. We did not observe CHIP-induced poly-ubiquitination of full-length Tau (2N4R), while both Tau fragments generated by caspase-2 cleavage (1–421 and 66–421) were readily modified (Fig. 6A). To determine whether this increased ubiquitination could be reproduced intracellularly, we transfected the three different Tau constructs into HEK293 cells together with ubiquitin and CHIP. We then measured the levels of total and ubiquitinated Tau by ELISA. Also in this system, the ratio of ubiquitinated over total Tau was significantly higher for both Tau fragments compared to full-length Tau, with ubiquitination of Tau 66–421 exceeding the signal obtained from Tau 1–421 (Fig. 6B). These data thus confirm the preferential CHIP-mediated ubiquitination of Tau fragments truncated at D421, which is further facilitated intracellularly by the additional truncation at D65.

To assess the degradation kinetics of Tau fragments in more detail, we co-transfected Tau 1–441, Tau 1–421 and Tau 66–421 respectively into HEK293 cells together with ubiquitin and CHIP. Treatment with cycloheximide (CHX) to block *de novo* protein synthesis revealed that the levels of both Tau fragments declined significantly faster than the

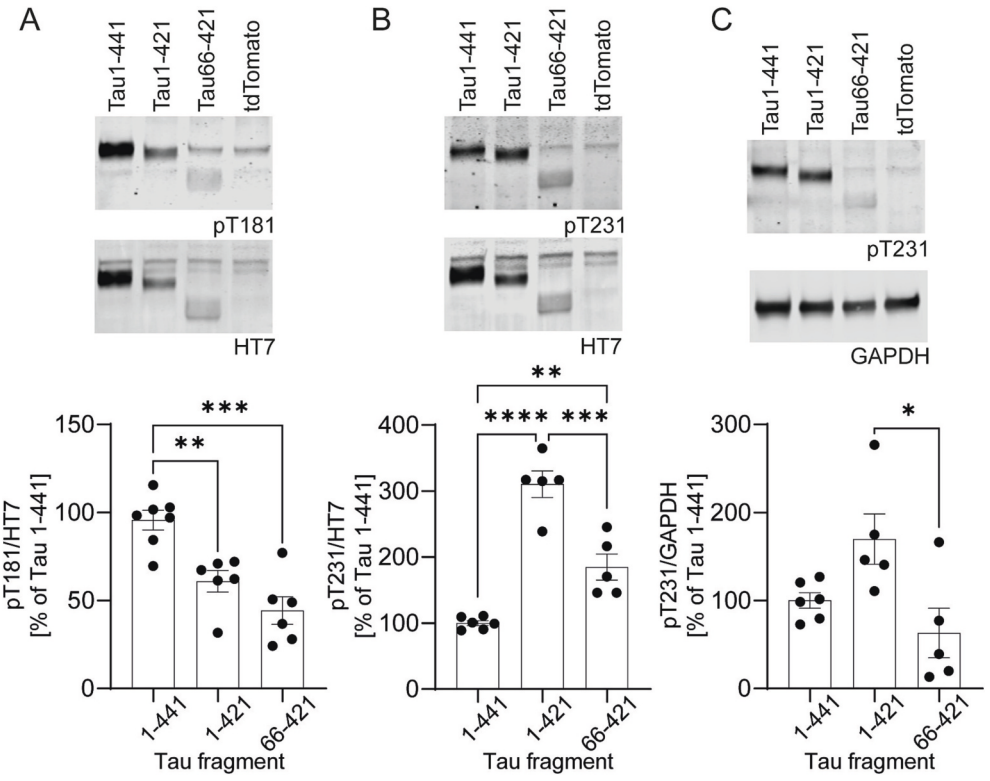

Fig. 4. Phosphorylation patterns are altered on Tau fragments compared to the full-length protein expressed *in vivo*.
(A) – (C) Western blot analyses of different disease-relevant Tau phosphorylation sites reveal altered phosphorylation patterns of Tau fragments compared to the full-length protein. n = 5–7 animals per group. Statistical significance was determined by one-way ANOVA: (A): $p < 0.0001$; (B): p < 0.0001; (C): $p < 0.05$), with Tukey's post-hoc comparisons test (****: p < 0.0001; ***: p < 0.001; **: p < 0.01; *: p < 0.05).

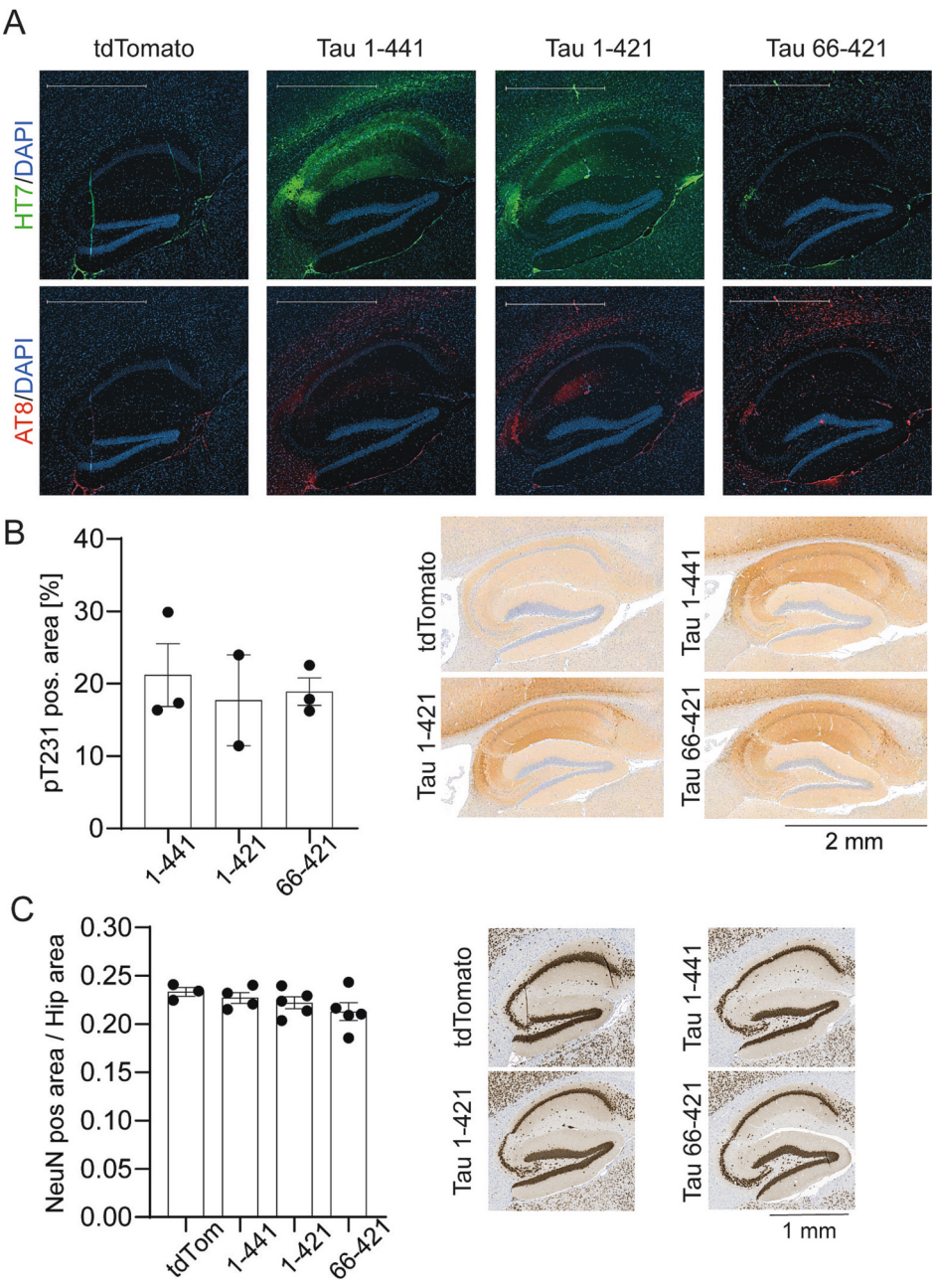

Fig. 5. Decreased Tau immunoreactivity without neuronal loss is observed in mice expressing Tau fragments.
(A) Analyses of total (HT7, green) and phospho-Tau (AT8, red) immunoreactivity in AAV-injected mouse hippocampi demonstrate low levels of total Tau protein in mice expressing Tau 66–421. HT7 immunoreactivity was strongest in Tau 1–441 expressing animals, Tau 1–421 yielded intermediate levels. Phospho-Tau immunoreactivity (AT8) was low in all experimental groups. tdTomato-expressing mice are included as a negative control. Scale bar: 1 mm, $n = 4$–5 animals per group, representative images are shown. (B) No difference in pT231-Tau immunoreactive hippocampal area was observed in mice overexpressing full-length Tau or Tau fragments. $n = 2$–3 animals. Statistical significance was determined by one-way ANOVA ($p = 0.8343$). (C) No difference in NeuN immunoreactive hippocampal area was observed in mice overexpressing full-length Tau or Tau fragments compared to the tdTomato-expressing control group. $n = 3$–5 animals. Statistical significance was determined by one-way ANOVA ($p = 0.3190$).

full-length protein. After 6 h of CHX treatment, levels of both Tau fragments were significantly lower than Tau 1–441 levels, confirming that increased CHIP-mediated ubiquitination also leads to increased degradation of Tau fragments (Fig. 6C). CHIP-mediated degradation may also be responsible for the low Tau fragment levels observed in our *in vivo* model, since we observed a strong interaction of endogenous CHIP with Tau fragments, but not full-length Tau by co-immunoprecipitation from mouse hippocampal lysates (Fig. 6D). Taken together these findings suggest that both *in vitro* and *in vivo*, CHIP preferentially interacts with Tau fragments truncated at D421, which may mediate their preferential degradation and lead to the low steady-state protein levels observed in our mouse model.

4. Discussion

Here we report the discovery of a novel caspase-2 cleavage site on the Tau protein at D65, which is efficiently processed *in vitro* and in cell culture, and we present evidence for the presence of D65-cleaved Tau in human brain samples. We furthermore show that caspase-2 is also capable of cleaving Tau at D421, thus generating a fragment truncated at both the N- and C- terminus. Previous studies reported cleavage of Tau by caspase-2 at D314 (Liu et al., 2019; Zhao et al., 2016), which was not found as a major site in our experiments. However, the published data were generated using the 0N4R Tau isoform, which lacks the N-terminal inserts harboring D65 (Zhao et al., 2016), potentially explaining the differences to our work with the 2N4R isoform. Our *in vitro* and cell-based cleavage analysis of Tau by caspase-2 suggests that D421 and D65 are major cleavage sites for isoforms that contain the first N-terminal insert, which is also supported by *in silico* predictions (Kumar et al., 2014).

Caspase-2 has been shown to mediate synaptic, cognitive, and motor deficits in mouse models of multiple neurodegenerative diseases, including AD and Huntington's disease (HD) (Carroll et al., 2011; Pozueta et al., 2013). Increased protein levels of caspase-2 were found in

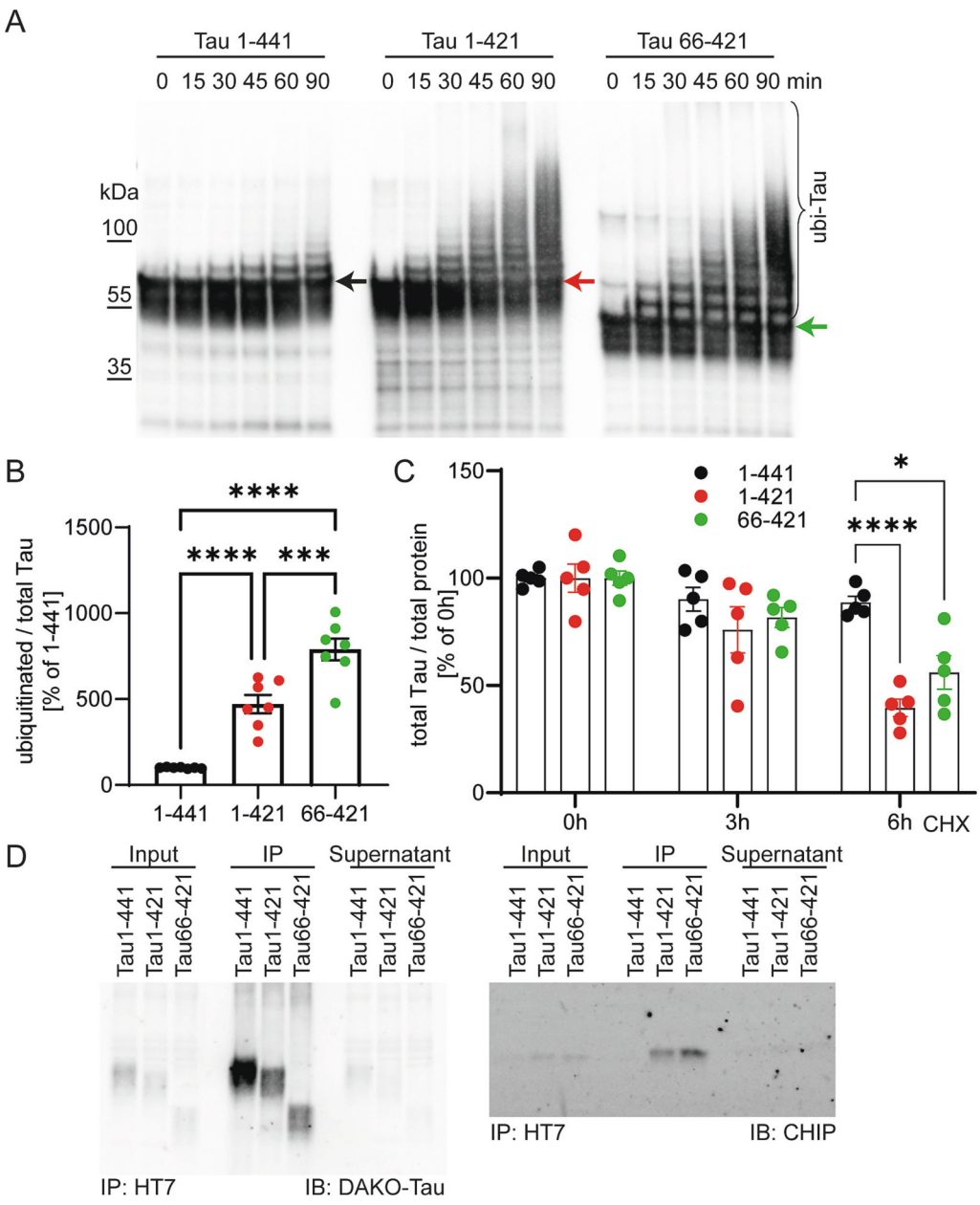

Fig. 6. Caspase-2 generated Tau fragments preferentially bind CHIP and show increased ubiquitination and degradation.
(A) Recombinant Tau 1–421 and 66–421 fragments, but not full-length Tau are readily ubiquitinated by CHIP *in vitro*. Ubiquitinated samples show a time-dependent increase in high-molecular weight species on the gel detected with a total Tau antibody (Abcam ab64193). The sizes for monomeric proteins are indicated by arrows (black: 1–441, green: 1–421, red: 66–421). (B) Co-transfection of CHIP, Tau and ubiquitin in HEK293 cells leads to increased ubiquitinated/total Tau ratios measured by ELISA for both Tau fragments compared to full-length Tau. Statistical significance was determined by one-way ANOVA ($p < 0.0001$), with Tukey's post-hoc comparisons test (****: $p < 0.0001$; ***: $p < 0.001$). (C) HEK293 cells were co-transfected with ubiquitin, CHIP and Tau and treated with cycloheximide (CHX) for the indicated amounts of time to block *de novo* protein synthesis. Tau levels were measured by ELISA and normalized to total protein content of the respective lysate. 6 h of CHX treatment revealed significantly lower levels of Tau fragments compared to the full-length protein, indicative of accelerated degradation. Statistical significance was determined by two-way ANOVA (time: $p < 0.0001$; Tau fragment: $p < 0.01$), with Tukey's post-hoc comparisons test (****: $p < 0.0001$; *: $p < 0.05$). (D) CHIP co-immunoprecipitates with Tau fragments, but not with full-length Tau in hippocampal lysates of AAV-injected mice. Representative Western blots of n = 3 independent experiments are shown.

brain tissue from AD and HD patients as well as cognitively impaired individuals (Liu et al., 2020, 2019; Shimohama et al., 1999), while mRNA levels of the enzyme appear unchanged (Hlynialuk et al., 2022). The upregulation of caspase-2 thereby is not necessarily linked to apoptosis, since non-apoptotic functions have been described for multiple caspases and neuronal caspase activity has been observed in the absence of acute cell death (Calignon et al., 2010; Ehrnhoefer et al., 2019; Li et al., 2010; Spires-Jones et al., 2008; Unsain and Barker, 2015).

Caspase-mediated Tau cleavage generates aggregation-prone fragments, however, their exact role in the pathogenesis of AD is controversial. On the one hand, the Tau D421 neoepitope is part of neurofibrillary tangles found in patient brain tissue (Jarero-Basulto et al., 2013; Rissman et al., 2004; Rohn, 2010) and a transgenic mouse model overexpressing the Tau 1–421 fragment exhibits severe neurological phenotypes (Kim et al., 2016). Furthermore, an antibody against D421-cleaved Tau immunodepletes seeding-competent high-molecular weight protein fractions isolated from human AD brain, suggesting that caspase-cleaved Tau is an important component of pathological Tau aggregates (Nicholls et al., 2017). On the other hand, the expression of a cleavage-resistant version (D421N) of the endogenous mouse Tau in a knock-in model also causes severe neurodegenerative phenotypes including Tau hyperphosphorylation, synaptic deficits and impaired memory (Biundo et al., 2017), suggesting that D421 proteolysis may also be important for normal neuronal physiology.

Studying the effects of AAV-mediated Tau expression on cognitive performance *in vivo*, only a slight deficit in the MWM was observed for mice expressing Tau 1–441. This is consistent with a previous study showing that the overexpression of human Tau in a murine tau knockout mouse leads to memory impairment (Goncalves et al., 2020), and human full-length Tau overexpression is also sufficient to induce neurodegeneration in Drosophila (Jackson et al., 2002). At the same time, all comparisons for Tau 1–441 with Tau fragments in our study are confounded by the strong differences in steady-state protein levels we observed *in vivo*, precluding a detailed analysis of toxicity and cognitive impairment for caspase-2 derived Tau fragments in our model. While strong RNA expression was observed for all constructs, immunofluorescent staining and Western blot analyses showed >50% lower total Tau protein levels for both Tau fragments compared to Tau 1–441.

Despite these low Tau protein fragment levels, we found that the ubiquitin E3 ligase CHIP preferentially co-immunoprecipitates with Tau 1–421 and Tau 66–421, and no interaction was observed for Tau 1–441. Published data demonstrating that CHIP interacts with Tau and that caspase cleavage may unmask novel binding sites for CHIP in its substrates are in agreement with this finding (Dolan and Johnson, 2010; Grelle et al., 2006; Ravalin et al., 2019). Together with our *in vitro* data demonstrating preferential ubiquitination and faster clearance of Tau fragments in the presence of CHIP, this suggests that Tau fragments may also be subject to a faster turnover *in vivo*, which would lower steady state protein levels and prevent aggregation as well as any potential appearance of cognitive deficits. The C-terminal degron sequence exposed in caspase-cleaved Tau is one of multiple such motifs discovered in recent years, each recognized by a specific ubiquitin ligase (Timms and Koren, 2020). The regulation of degron efficiency through PTMs is also not unique to CHIP and may be a more general mechanism for tissue-specific, disease-specific or aging-related differential protein degradation (Timms and Koren, 2020).

Previous studies have demonstrated that either knockdown or ablation of CHIP lead to the accumulation of hyperphosphorylated Tau *in vivo* (Dickey et al., 2006). However, the connection to Tau aggregation is less clear, since no aggregation of WT mouse or transgenic human Tau was observed in Tau P301L mice ablated for CHIP (Dickey et al., 2006). Despite the low total Tau protein levels, we observed a relative increase in pT231-modified Tau in mice expressing Tau 1–421 or Tau 66–421, and immunoreactivity with a pT231-Tau antibody was equal in brain sections from mice expressing full-length Tau or the two different Tau fragments. Since proteolytic cleavage is not necessary in our model, this suggests that either the fragments themselves undergo altered phosphorylation or alternatively that phosphorylated Tau fragments are cleared less efficiently than their non- phosphorylated counterparts.

Both CHIP and D421-cleaved Tau have been found in neuronal inclusions in the brains of human patients with AD or other tauopathies (Jarero-Basulto et al., 2013; Petrucelli et al., 2004; Ravalin et al., 2019; Rissman et al., 2004). Recent evidence furthermore points towards a progressive dysfunction of CHIP in AD brain, which may promote the abnormal accumulation of Tau fragments (Ravalin et al., 2019). A better understanding of the pathological cascade leading to the accumulation of Tau and its fragments, and of the age- or pathology-related dysfunction of clearance mechanisms may thus ultimately lead to the identification of tractable therapeutic targets for AD and other tauopathies.

Supplementary data to this article can be found online at https://doi.org/10.1016/j.nbd.2023.106126.

Author contributions

LR performed *in vivo* and *ex vivo* experiments and coordinated co-author contributions. FM performed the analysis of behavioral experiments, MB performed *in vitro* cleavage experiments, AB performed ThT assays and performed *in vivo* work. EEH performed image analysis of IHC data, PH, IB and MS contributed MS data, JS, MS and CK contributed *in situ* hybridization and IHC data, JM, DCS and CP contributed Tau ubiquitination data. JK and PR contributed to Tau expression analyses. LG provided scientific input and advice. MF supervised *in vivo* experiments, DEE performed immunoprecipitation experiments, conceived and supervised the project and wrote the first draft of the manuscript. All authors contributed to data discussion and interpretation, critically revised or contributed to the manuscript. All authors read and approved the final manuscript.

Declaration of Competing Interest

JM, MS, JK, PR, LG, CP and CK are employees of AbbVie, LR, DCS and DEE joined AbbVie as employees during the study. JS was an employee of AbbVie at the time of the study. FM and MF are employees of the German Center for Neurodegenerative Diseases (DZNE), their contributions to the study were funded by BioMed X GmbH. PH, MS and IB are employees of EMBL, their contributions to the study were funded by BioMed X GmbH. EEH is an employee of BioMed X GmbH, MB and AB were employees of BioMed X GmbH at the time of the study (a contract research agreement was funded by AbbVie). The design, study conduct, and financial support for this research were provided by AbbVie. AbbVie participated in the interpretation of data, review, and approval of the publication.

Data availability

Mass spectrometry data were previously deposited to the ProteomeXchange Consortium via the PRIDE repository with the identifier PXD017065.

Acknowledgements

The study was funded by a contract research agreement between AbbVie Inc. (North Chicago, IL, USA) and BioMed X GmbH. We thank Dr. Kim Remans and Dr. Jacob Scheurich at the EMBL protein purification core facility for the expression and purification of recombinant Tau proteins, which was funded by BioMed X GmbH. We are also thankful to Andrea Baral and Stefanie Poll at the German Center for Neurodegenerative diseases (DZNE) for their assistance with animal husbandry and training of *in vivo* techniques (funded by BioMed X GmbH).

References

Baliga, B.C., Read, S.H., Kumar, S., 2004. The biochemical mechanism of caspase-2 activation. Cell Death Differ. 11, 1234–1241. https://doi.org/10.1038/sj.cdd.4401492.

Basurto-Islas, G., Luna-Muñoz, J., Guillozet-Bongaarts, A.L., Binder, L.I., Mena, R., García-Sierra, F., 2008. Accumulation of aspartic Acid421- and glutamic Acid391-cleaved tau in neurofibrillary tangles correlates with progression in Alzheimer disease. J. Neuropathol. Exp. Neurol. 67, 470–483. https://doi.org/10.1097/nen.0b013e31817275c7.

Behrendt, A., Bichmann, M., Ercan-Herbst, E., Haberkant, P., Schondorf, D.C., Wolf, M., Fahim, S.A., Murolo, E., Ehrnhoefer, D.E., 2019. Asparagine endopeptidase cleaves tau at N167 after uptake into microglia. Neurobiol. Dis. 130, 104518 https://doi.org/10.1016/j.nbd.2019.104518.

Biundo, F., d'Abramo, C., Tambini, M.D., Zhang, H., Prete, D.D., Vitale, F., Giliberto, L., Arancio, O., D'Adamio, L., 2017. Abolishing Tau cleavage by caspases at aspartate (421) causes memory/synaptic plasticity deficits and pre-pathological tau alterations. Transl. Psychiatry 7, e1198. https://doi.org/10.1038/tp.2017.165.

Calignon, A., Fox, L.M., Pitstick, R., Carlson, G.A., Bacskai, B.J., Spires-Jones, T.L., Hyman, B.T., 2010. Caspase activation precedes and leads to tangles. Nature 464, 1201–1204. https://doi.org/10.1038/nature08890.

Carroll, J.B., Southwell, A.L., Graham, R.K., Lerch, J.P., Ehrnhoefer, D.E., Cao, L.P., Zhang, W.N., Deng, Y., Bissada, N., Henkelman, R.M., Hayden, M.R., 2011. Mice lacking caspase-2 are protected from behavioral changes, but not pathology, in the YAC128 model of Huntington disease. Mol. Neurodegener. 6, 59. https://doi.org/10.1186/1750-1326-6-59.

Dawson, H.N., Ferreira, A., Eyster, M.V., Ghoshal, N., Binder, L.I., Vitek, M.P., 2001. Inhibition of neuronal maturation in primary hippocampal neurons from tau deficient mice. J. Cell Sci. 114, 1179–1187. https://doi.org/10.1242/jcs.114.6.1179.

Dickey, C.A., Yue, M., Lin, W.-L., Dickson, D.W., Dunmore, J.H., Lee, W.C., Zehr, C., West, G., Cao, S., Clark, A.M.K., Caldwell, G.A., Caldwell, K.A., Eckman, C., Patterson, C., Hutton, M., Petrucelli, L., 2006. Deletion of the ubiquitin ligase CHIP leads to the accumulation, but not the aggregation, of both endogenous Phospho- and Caspase-3-cleaved tau species. J. Neurosci. 26, 6985–6996. https://doi.org/10.1523/jneurosci.0746-06.2006.

Dolan, P.J., Johnson, G.V., 2010. A caspase cleaved form of tau is preferentially degraded through the autophagy pathway. J. Biol. Chem. 285, 21978–21987. https://doi.org/10.1074/jbc.m110.110940.

Ehrnhoefer, D.E., Skotte, N.H., Reinshagen, J., Qiu, X., Windshugel, B., Jaishankar, P., Ladha, S., Petina, O., Khankischpur, M., Nguyen, Y.T.N., Caron, N.S., Razeto, A., Rheda, M.M.Z., Deng, Y., Huynh, K.T., Wittig, I., Gribbon, P., Renslo, A.R., Geffken, D., Gul, S., Hayden, M.R., 2019. Activation of Caspase-6 is promoted by a mutant huntingtin fragment and blocked by an allosteric inhibitor compound. Cell Chem Biol 26 (1295–1305), e6. https://doi.org/10.1016/j.chembiol.2019.07.001.

Ercan-Herbst, E., Ehrig, J., Schondorf, D.C., Behrendt, A., Klaus, B., Ramos, B.G., Oriol, N.P., Weber, C., Ehrnhoefer, D.E., 2019. A post-translational modification signature defines changes in soluble tau correlating with oligomerization in early stage Alzheimer's disease brain. Acta Neuropathologica Commun. 7, 192. https://doi.org/10.1186/s40478-019-0823-2.

Franken, H., Mathieson, T., Childs, D., Sweetman, G.M.A., Werner, T., Tögel, I., Doce, C., Gade, S., Bantscheff, M., Drewes, G., Reinhard, F.B.M., Huber, W., Savitski, M.M., 2015. Thermal proteome profiling for unbiased identification of direct and indirect drug targets using multiplexed quantitative mass spectrometry. Nat. Protoc. 10, 1567–1593. https://doi.org/10.1038/nprot.2015.101.

Gamblin, T.C., Chen, F., Zambrano, A., Abraha, A., Lagalwar, S., Guillozet, A.L., Lu, M., Fu, Y., Garcia-Sierra, F., LaPointe, N., Miller, R., Berry, R.W., Binder, L.I., Cryns, V.L., 2003. Caspase cleavage of tau: linking amyloid and neurofibrillary tangles in Alzheimer's disease. Proc. National Acad. Sci. 100, 10032–10037. https://doi.org/10.1073/pnas.1630428100.

Goncalves, R.A., Wijesekara, N., Fraser, P.E., Felice, F.G.D., 2020. Behavioral abnormalities in knockout and humanized tau mice. Front. Endocrinol. 11, 124. https://doi.org/10.3389/fendo.2020.00124.

Grelle, G., Kostka, S., Otto, A., Kersten, B., Genser, K.F., Muller, E.C., Walter, S., Boddrich, A., Stelzl, U., Hanig, C., Volkmer-Engert, R., Landgraf, C., Alberti, S., Hohfeld, J., Strodicke, M., Wanker, E.E., 2006. Identification of VCP/p97, carboxyl terminus of Hsp70-interacting protein (CHIP), and amphiphysin II interaction partners using membrane-based human proteome arrays. Mol. Cell. Proteomics 5, 234–244. https://doi.org/10.1074/mcp.m500198-mcp200.

Guillozet-Bongaarts, A.L., Garcia-Sierra, F., Reynolds, M.R., Horowitz, P.M., Fu, Y., Wang, T., Cahill, M.E., Bigio, E.H., Berry, R.W., Binder, L.I., 2005. Tau truncation during neurofibrillary tangle evolution in Alzheimer's disease. Neurobiol. Aging 26, 1015–1022. https://doi.org/10.1016/j.neurobiolaging.2004.09.019.

Hlynialuk, C., Kemper, L., Leinonen-Wright, K., Petersen, R.C., Ashe, K., Smith, B., 2022. Caspase-2 mRNA levels are not elevated in mild cognitive impairment, Alzheimer's disease, Huntington's disease, or Lewy body dementia. PLoS One 17, e0274784. https://doi.org/10.1371/journal.pone.0274784.

Horowitz, P.M., Patterson, K.R., Guillozet-Bongaarts, A.L., Reynolds, M.R., Carroll, C.A., Weintraub, S.T., Bennett, D.A., Cryns, V.L., Berry, R.W., Binder, L.I., 2004. Early N-terminal changes and caspase-6 cleavage of tau in Alzheimer's disease. J. Neurosci. 24, 7895–7902. https://doi.org/10.1523/jneurosci.1988-04.2004.

Jackson, G.R., Wiedau-Pazos, M., Sang, T.K., Wagle, N., Brown, C.A., Massachi, S., Geschwind, D.H., 2002. Human wild-type tau interacts with wingless pathway components and produces neurofibrillary pathology in Drosophila. Neuron 34, 509–519. https://doi.org/10.1016/s0896-6273(02)00706-7.

Jarero-Basulto, J.J., Luna-Munoz, J., Mena, R., Kristofikova, Z., Ripova, D., Perry, G., Binder, L.I., Garcia-Sierra, F., 2013. Proteolytic cleavage of polymeric tau protein by caspase-3: implications for Alzheimer disease. J. Neuropathol. Exp. Neurol. 72, 1145–1161. https://doi.org/10.1097/nen.0000000000000013.

Jeganathan, S., Bergen, M., Brutlach, H., Steinhoff, H.J., Mandelkow, E., 2006. Global hairpin folding of tau in solution. Biochemistry-us 45, 2283–2293. https://doi.org/10.1021/bi0521543.

Kim, Y., Choi, H., Lee, W., Park, H., Kam, T.I., Hong, S.H., Nah, J., Jung, S., Shin, B., Lee, H., Choi, T.Y., Choo, H., Kim, K.K., Choi, S.Y., Kayed, R., Jung, Y.K., 2016. Caspase-cleaved tau exhibits rapid memory impairment associated with tau oligomers in a transgenic mouse model. Neurobiol. Dis. 87, 19–28. https://doi.org/10.1016/j.nbd.2015.12.006.

Kumar, S., Raam, B.J., Salvesen, G.S., Cieplak, P., 2014. Caspase cleavage sites in the human proteome: CaspDB, a database of predicted substrates. PLoS One 9, e110539. https://doi.org/10.1371/journal.pone.0110539.

Li, Z., Jo, J., Jia, J.M., Lo, S.C., Whitcomb, D.J., Jiao, S., Cho, K., Sheng, M., 2010. Caspase-3 activation via mitochondria is required for long-term depression and AMPA receptor internalization. Cell 141, 859–871. https://doi.org/10.1016/j.cell.2010.03.053.

Liu, P., Smith, B.R., Huang, E.S., Mahesh, A., Vonsattel, J.P.G., Petersen, A.J., Gomez-Pastor, R., Ashe, K.H., 2019. A soluble truncated tau species related to cognitive dysfunction and caspase-2 is elevated in the brain of Huntington's disease patients. Acta Neuropathologica Commun. 7, 111. https://doi.org/10.1186/s40478-019-0764-9.

Liu, P., Smith, B.R., Montonye, M.L., Kemper, L.J., Leinonen-Wright, K., Nelson, K.M., Higgins, L., Guerrero, C.R., Markowski, T.W., Zhao, X., Petersen, A.J., Knopman, D. S., Petersen, R.C., Ashe, K.H., 2020. A soluble truncated tau species related to cognitive dysfunction is elevated in the brain of cognitively impaired human individuals. Sci. Report. 10, 3869. https://doi.org/10.1038/s41598-020-60777-x.

Mead, E., Kestoras, D., Gibson, Y., Hamilton, L., Goodson, R., Jones, S., Eversden, S., Davies, P., O'Neill, M., Hutton, M., Szekeres, P., Wolak, J., 2016. Halting of caspase activity protects tau from MC1-conformational change and aggregation. J. Alzheimers Dis. 54, 1521–1538. https://doi.org/10.3233/jad-150960.

Morris, R., 1984. Developments of a water-maze procedure for studying spatial learning in the rat. J. Neurosci. Methods 11, 47–60. https://doi.org/10.1016/0165-0270(84)90007-4.

Myrum, C., Baumann, A., Bustad, H.J., Flydal, M.I., Mariaule, V., Alvira, S., Cuéllar, J., Haavik, J., Soulé, J., Valpuesta, J.M., Márquez, J.A., Martinez, A., Bramham, C.R., 2015. Arc is a flexible modular protein capable of reversible self-oligomerization. Biochem. J. 468, 145–158. https://doi.org/10.1042/bj20141446.

Nicholls, S.B., DeVos, S.L., Commins, C., Nobuhara, C., Bennett, R.E., Corjuc, D.L., Maury, E., Eftekharzadeh, B., Akingbade, O., Fan, Z., Roe, A.D., Takeda, S., Wegmann, S., Hyman, B.T., 2017. Characterization of TauC3 antibody and demonstration of its potential to block tau propagation. PLoS One 12, e0177914. https://doi.org/10.1371/journal.pone.0177914.

Paul, I., Ghosh, M.K., 2014. The E3 ligase CHIP: insights into its structure and regulation. Biomed. Res. Int. 2014, 918183 https://doi.org/10.1155/2014/918183.

Petrucelli, L., Dickson, D., Kehoe, K., Taylor, J., Snyder, H., Grover, A., Lucia, M.D., McGowan, E., Lewis, J., Prihar, G., Kim, J., Dillmann, W.H., Browne, S.E., Hall, A., Voellmy, R., Tsuboi, Y., Dawson, T.M., Wolozin, B., Hardy, J., Hutton, M., 2004. CHIP and Hsp70 regulate tau ubiquitination, degradation and aggregation. Hum. Mol. Genet. 13, 703–714. https://doi.org/10.1093/hmg/ddh083.

Pozueta, J., Lefort, R., Ribe, E.M., Troy, C.M., Arancio, O., Shelanski, M., 2013. Caspase-2 is required for dendritic spine and behavioural alterations in J20 APP transgenic mice. Nat. Commun. 4, 1939. https://doi.org/10.1038/ncomms2927.

Quinn, J.P., Corbett, N.J., Kellett, K.A.B., Hooper, N.M., 2018. Tau proteolysis in the pathogenesis of Tauopathies: neurotoxic fragments and novel biomarkers. J. Alzheimers Dis. 63, 13–33. https://doi.org/10.3233/jad-170959.

Ravalin, M., Theofilas, P., Basu, K., Opoku-Nsiah, K.A., Assimon, V.A., Medina-Cleghorn, D., Chen, Y.F., Bohn, M.F., Arkin, M., Grinberg, L.T., Craik, C.S., Gestwicki, J.E., 2019. Specificity for latent C termini links the E3 ubiquitin ligase CHIP to caspases. Nat. Chem. Biol. 15, 786–794. https://doi.org/10.1038/s41589-019-0322-6.

Rissman, R.A., Poon, W.W., Blurton-Jones, M., Oddo, S., Torp, R., Vitek, M.P., LaFerla, F. M., Rohn, T.T., Cotman, C.W., 2004. Caspase-cleavage of tau is an early event in Alzheimer disease tangle pathology. J. Clin. Invest. 114, 121–130. https://doi.org/10.1172/jci20640.

Rohn, T.T., 2010. The role of caspases in Alzheimer's disease; potential novel therapeutic opportunities. Apoptosis 15, 1403–1409. https://doi.org/10.1007/s10495-010-0463-2.

Shimohama, S., Tanino, H., Fujimoto, S., 1999. Changes in caspase expression in Alzheimer's disease: comparison with development and aging. Biochem. Bioph. Res. Co 256, 381–384. https://doi.org/10.1006/bbrc.1999.0344.

Spires-Jones, T.L., Calignon, A.D., Matsui, T., Zehr, C., Pitstick, R., Wu, H.Y., Osetek, J. D., Jones, P.B., Bacskai, B.J., Feany, M.B., Carlson, G.A., Ashe, K.H., Lewis, J., Hyman, B.T., 2008. In vivo imaging reveals dissociation between caspase activation and acute neuronal death in tangle-bearing neurons, 28, 862–867. https://doi.org/10.1523/jneurosci.3072-08.2008.

Strooper, B.D., 2010. Proteases and proteolysis in Alzheimer disease: a multifactorial view on the disease process. Physiol. Rev. 90, 465–494. https://doi.org/10.1152/physrev.00023.2009.

Timms, R.T., Koren, I., 2020. Tying up loose ends: the N-degron and C-degron pathways of protein degradation. Biochem. Soc. T 48, 1557–1567. https://doi.org/10.1042/bst20191094.

Unsain, N., Barker, P.A., 2015. New views on the misconstrued: executioner caspases and their diverse non-apoptotic roles. Neuron 88, 461–474. https://doi.org/10.1016/j.neuron.2015.08.029.

Vorhees, C.V., Williams, M.T., 2006. Morris water maze: procedures for assessing spatial and related forms of learning and memory. Nat. Protoc. 1, 848–858. https://doi.org/10.1038/nprot.2006.116.

Wang, Y., Mandelkow, E., 2016. Tau in physiology and pathology. Nat. Rev. Neurosci. 17, 5–21. https://doi.org/10.1038/nrn.2015.1.

Wesseling, H., Mair, W., Kumar, M., Schlaffner, C.N., Tang, S., Beerepoot, P., Fatou, B., Guise, A.J., Cheng, L., Takeda, S., Muntel, J., Rotunno, M.S., Dujardin, S., Davies, P., Kosik, K.S., Miller, B.L., Berretta, S., Hedreen, J.C., Grinberg, L.T., Seeley, W.W., Hyman, B.T., Steen, H., Steen, J.A., 2020. Tau PTM profiles identify patient heterogeneity and stages of Alzheimer's disease. Cell 183 (1699–1713), e13. https://doi.org/10.1016/j.cell.2020.10.029.

Zhao, X., Kotilinek, L.A., Smith, B., Hlynialuk, C., Zahs, K., Ramsden, M., Cleary, J., Ashe, K.H., 2016. Caspase-2 cleavage of tau reversibly impairs memory. Nat. Med. 22, 1268–1276. https://doi.org/10.1038/nm.4199.